Top Catal (2015) 58:314–324
DOI 10.1007/s11244-015-0372-2

ORIGINAL PAPER

Facile Styrene Epoxidation with H_2O_2 over Novel Niobium Containing Cage Type Mesoporous Silicate, Nb-KIT-5

Anand Ramanathan · Rajamanickam Maheswari · Bala Subramaniam

Published online: 3 March 2015

Abstract Niobium has been incorporated into cage-like ordered mesoporous KIT-5, a cubic close-packed (*Fm3m*) structured silica, for the first time by a direct hydrothermal synthesis method. Small-angle X-ray scattering spectra and nitrogen physisorption results confirm the formation of the KIT-5 structure. The incorporation of Nb and its coordination were confirmed by techniques such as elemental analysis, diffuse reflectance UV–Vis, Raman, HR-SEM and NH_3-TPD. When tested as epoxidation catalyst for styrene with H_2O_2, Nb-KIT-5 mainly yielded (1,2-dimethoxyethyl) benzene with methanol as solvent. It also showed better catalytic activity compared to other mesostructured catalysts such as Nb-KIT-6 and Nb-SBA-15.

Keywords KIT-5 · Niobium · Lewis acid · Epoxidation · Styrene

Electronic Supplementary Material The online version of this article (doi:10.1007/s11244-015-0372-2) contains supplementary material, which is available to authorized users.

A. Ramanathan · R. Maheswari · B. Subramaniam
Center for Environmentally Beneficial Catalysis, The University of Kansas, Lawrence, KS 66047, USA

R. Maheswari
Department of Chemistry, Anna University, Chennai 600025, India

B. Subramaniam (✉)
Department of Chemical and Petroleum Engineering, The University of Kansas, Lawrence, KS 66045, USA
e-mail: bsubramaniam@ku.edu

1 Introduction

In recent years, heterogeneous titanium- and niobium-based materials have attracted increased attention as olefin epoxidation catalysts [1, 2]. Somma et al. reported on cyclohexene epoxidation with H_2O_2 as oxidant over micro-, meso- and macroporous Nb/SiO_2 catalysts and concluded that Nb/SiO_2 samples prepared by aerogel method (using supercritical drying of solvent) are truly heterogeneous and those prepared by sol–gel techniques (with conventional solvent drying) lead to leaching of Nb species [3]. In contrast, niobium–silicon mixed oxide nanocomposites prepared by sol gel technique are reported to be stable and active for cyclooctene epoxidation [4]. Grafting and/or deposition of *bis*(cyclopentadienyl)niobium(IV) dichloride $[Nb(Cp)_2Cl_2]$ onto silica supports was also shown to create sites that are active for epoxidation of various substrates such as cycloalkanes, limonene, carveol, α-terpineol, isopulegol, carvotanacetol, carvone and unsaturated fatty acid methyl esters [5–7]. Even though hot-filtration tests did not show any evidence of activity in the filtered liquid phase, these grafted materials nevertheless lose catalytic activity after multiple recycle runs [8].

Direct incorporation of Nb(V) species on to ordered mesoporous silicates (OMS) such as MCM-41 was shown to yield a stable catalyst for cyclohexene oxidation with H_2O_2 as oxidant [9]. In contrast, V and Ti are found to leach out from MCM-41 supports [9]. While the Lewis acid sites created by niobium incorporation promote epoxide formation, the Brønsted acid sites catalyze ring opening of epoxide by hydrolysis [10]. We recently reported the synthesis of Nb-KIT-6 (*Ia3d* type structure) in which Nb was predominantly incorporated in the framework. The Nb-KIT-6 materials possess both Lewis and Brønsted acid sites which are tunable with Nb loading [11]. Indeed, for liquid

phase ethylene epoxidation over Nb-KIT-6 with H_2O_2 as oxidant, we observed both the epoxide and ring-opened products [12].

KIT-5 is a cage type 3D cubic mesoporous silicate with *Fm3m* type structure [13]. Transition metal ions incorporated in KIT-5 materials were recently reported to show higher catalytic activity compared to their incorporation in either 1D or 2D mesoporous structures [14–17] such as MCM-41 and SBA-15. In this work, we have successfully incorporated Nb into the KIT-5 framework without altering the synthesis procedure used for obtaining pure siliceous KIT-5. Comprehensive characterization of the structural properties and the nature of incorporation of the Nb species are presented. The Nb-KIT-5 materials are shown to provide excellent activity and stability for styrene epoxidation compared to Nb containing KIT-6, SBA-15, MCM-48 and MCM-41 type catalysts.

2 Experimental

2.1 Synthesis of Nb-KIT-5

The synthesis of Nb-KIT-5 materials with different molar ratios of Si and Nb in the synthesis mixture (n_{Si}/n_{Nb}) was achieved using a commercial nonionic triblock copolymer Pluronic F127 (Sigma) as a structure directing agent in an acidic medium similar to that of W-KIT-5 [18].

In a typical synthesis, Pluronic F127 (3.6 g, Sigma) was dissolved in HCl (0.4 M, 180 ml, Fisher) at 45 °C in a HDPE bottle with PP screw closure, followed by quick addition of tetraethyl orthosilicate (16.9 g, TEOS 98 %, Acros Organics) and required amounts of niobium(V) chloride (Strem, 99+ %). The mixture was stirred at 45 °C for 18–20 h and then heated at 98 °C for 24–48 h under static conditions in a Teflon-lined autoclave. The solid product was filtered without washing, dried and calcined in a muffle furnace (Thermo Scientific, Model No.:BF51866A-1) in flowing air (50 ml min^{-1} g_{sample}^{-1}) at 550 °C for 5 h. The resulting solids are denoted as Nb-KIT-5(x) where x represents the molar Si/Nb ratio in the synthesis gel.

2.2 Characterization of Nb-KIT-5

The prepared materials were characterized by a comprehensive set of complementary analytical tools such as small angle X-ray scattering, XRD, N_2 physisorption, ICP-OES elemental analysis, diffuse reflectance UV–Vis spectroscopy, transmission electron microscopy (TEM, SEM), Raman spectroscopy, temperature programmed desorption of ammonia (NH_3-TPD), temperature programmed reduction (H_2-TPR) and FTIR of adsorbed pyridine. Details of these techniques are given in our recent publication [11] and also summarized in the ESI.

2.3 Nb-KIT-5 Catalyzed Styrene Epoxidation

In a typical experiment, 2 mmol of styrene (99 %, ACROS Organics), 4 mmol of H_2O_2 (50 % aqueous solution, Fisher) and 3 ml methanol (99.8 %, Sigma-Aldrich) as solvent were added to a two-necked round bottom flask of 25 ml capacity equipped with a magnetic stirrer (Octagon Spinbar, 12.7 × 8 mm), thermometer and reflux condenser. Then required amounts of catalysts were charged to the reactor and heated to a desired temperature on a hot plate equipped with a magnetic stirrer and temperature controller (IKA Works, Model No. 9016401) at a stirring speed of 700 rpm. The reaction was monitored by withdrawing samples at regular intervals (typically 1, 3 and 6 h) and analyzed on a gas chromatograph (Agilent 7890A) with a capillary column (HP-1, 30 m × 0.32 mm, 0.25 μm) using a FID. The products were confirmed by matching retention times of authentic samples as well as by GC–MS (Agilent 5975C). The conversion and product selectivity were estimated as follows based on GC analysis of the products using an external standard method.

$$X_{styrene} = \frac{[styrene]_0 - [styrene]_t}{[styrene]_t}$$

$$S_{product} = \frac{[product]_t}{X_{styrene}} \times 100$$

Under our reaction conditions, both external and intraparticle mass transfer limitations are insignificant based on established criteria (see Table S1 in ESM).

3 Results and Discussion

3.1 Characterization of Nb-KIT-5

Three well resolved peaks at 2θ values of 0.77, 0.85 and 1.20°, attributed to the (111), (200) and (220) planes of cubic *Fm3m* structure respectively [13, 18–20] are observed in the SAXS patterns of Si-KIT-5 and Nb-KIT-5 materials (Fig. 1). The observed *d* spacings and the unit cell parameter (a_0 =19.8–20.2 nm) calculated using $a_0 = d_{111}\sqrt{3}$, are similar to those reported for KIT-5 materials (a_0 =18.9–20.6 nm) [16, 18, 21]. The higher order peaks were not resolved in Nb-KIT-5(10), which has the highest Nb content (10 wt%) among the prepared materials. In addition, a drastic decrease in the intensity of the (111) peak was also noted for the Nb-KIT-5(10) material. This could be due to structural distortion caused by progressively increased incorporation of niobium species in the KIT-5 silica lattice at higher Nb loadings, which is also

verified by an increase in the unit cell parameter (a_0) in all the samples (see Table 1) [16, 18, 21]. Elemental analyses of the Nb-KIT-5 samples confirm a close match of the Si/Nb ratio present in the synthesis gel (Table 1). This also indicates that Nb can be incorporated into KIT-5 framework by direct synthesis without any adjustment of the synthesis composition of Si-KIT-5. In contrast, incorporation of metal ions such as Al [17], Co [15] and Ti [16] requires adjustment of the pH of the synthesis gel.

High-angle XRD of Nb-KIT-5 samples (Figure S1 in ESM) shows a lone broad peak around 2θ value between 15 and 25°, attributed to amorphous silica. No characteristic reflections of crystalline Nb_2O_5 are detectable even in Nb-KIT-5(10) sample with the highest Nb content. Such an observation has also been noted for other Nb-containing silicates such as Nb-KIT-6 [11], Nb-SBA-15 [22] and Nb-doped silica [23] suggesting that any niobium oxide present may be amorphous.

The absence of crystalline Nb_2O_5 was further confirmed from diffuse reflectance UV–Vis spectra (Fig. 2). All the Nb-KIT-5 samples show a well-defined absorption peak near 195 nm and a less prominent shoulder around 235–240 nm without any characteristic band for crystalline Nb_2O_5 [11]. These peaks may be deconvoluted to yield three peaks similar to those observed for Nb-KIT-6 [11], and is depicted in Fig. S2 in ESM. For samples with higher Nb loading (10 wt% Nb), these peaks are observed at 195, 219 and 248 nm. At lower Nb loadings, the 219 and 248 nm peaks are blue shifted to 200 and 230 nm, respectively. The absorption band at 195–220 nm is associated with O → NbO_4 LMCT [11, 24–27] and the band around 230–250 nm is assigned to oligomeric NbO_4

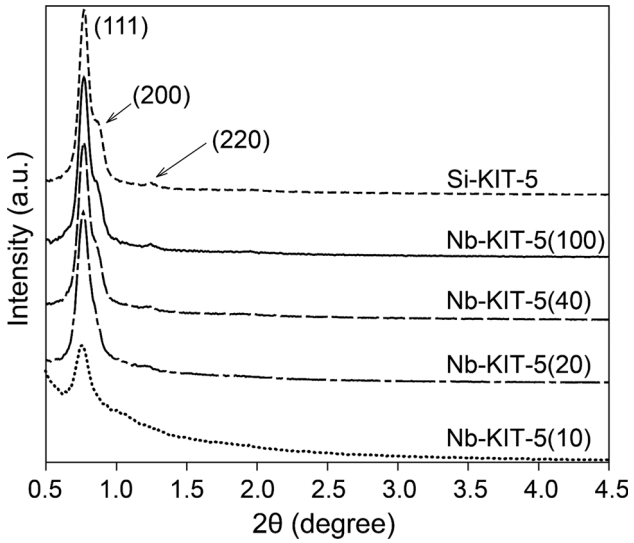

Fig. 1 Small-angle X-ray scattering (SAXS) analysis of Nb-KIT-5 (Si/Nb ratio) compared with Si-KIT-5

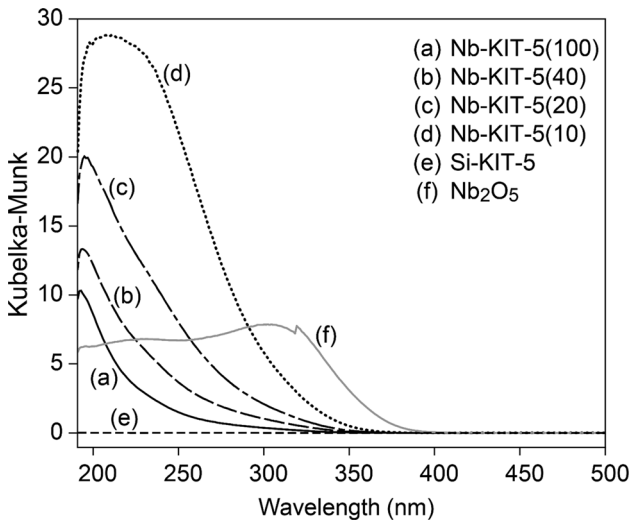

Fig. 2 Diffuse reflectance UV–Vis spectra of Nb-KIT-5(Si/Nb) samples compared with bulk Nb_2O_5

Table 1 Physicochemical properties of calcined NbKIT-5(Si/Nb)

KIT-5 (Si/Nb)[a]	Si/Nb[b]	Nb (wt%)[b]	a_0 (nm)[c]	S_{BET} (m^2 g^{-1})[d]	V_{tp}(cm^3 g^{-1})[e]	V_{mp} (cm^3 g^{-1})[f]	$d_{P,\ NLDFT}$ (nm)[g]
Si-KIT-5	–	–	19.8	1036	0.69	0.30	8.5
Nb-KIT-5(100)	106	1.4	19.8	1022	0.69	0.30	8.8
Nb-KIT-5(40)	42	3.3	19.8	978	0.65	0.21	8.8
Nb-KIT-5(20)	23	5.6	19.8	936	0.64	0.15	8.8
Nb-KIT-5(10)	11	10	20.2	810	0.81	0.06	8.8

[a] Molar ratio in the synthesis gel

[b] Actual molar ratio in sample determined by ICP-OES

[c] $a_0 = d_{111}\sqrt{3}$

[d] S_{BET} = specific surface area determined using Brunauer–Emmett–Teller (BET) equation from adsorption isotherm at P/P_0 between 0.01 and 0.25

[e] Vt_P = total pore volume at 0.98 P/P_0

[f] Vm_P = micropore volume by t-plot method, [g] $d_{P,NLDFT}$ = cage diameter determined using NLDFT kernel developed for silica exhibiting cylindrical/spherical pore geometry

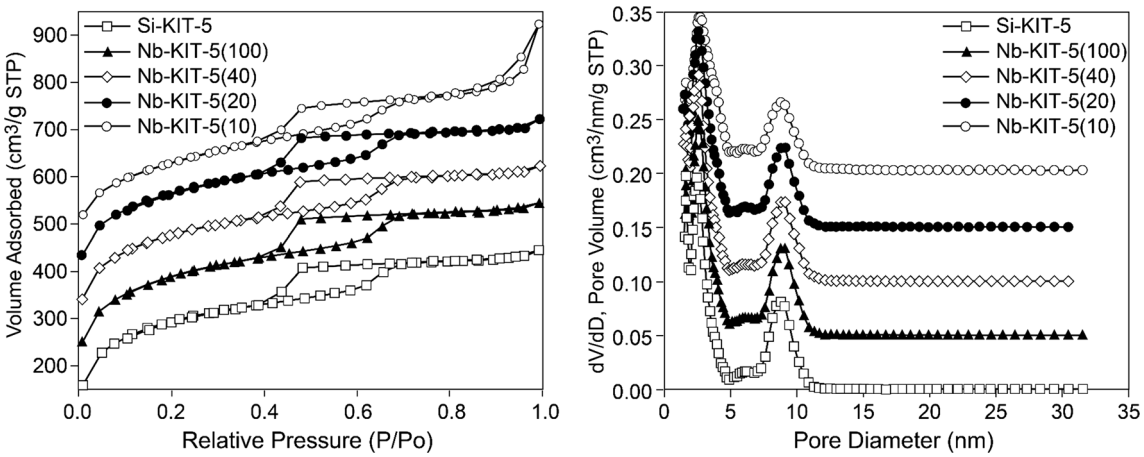

Fig. 3 N_2 sorption isotherms of Nb-KIT-5 samples (*left*) and their pore size distribution (*right*) determined using NLDFT adsorption branch kernel developed for silica exhibiting cylindrical/spherical pore geometry

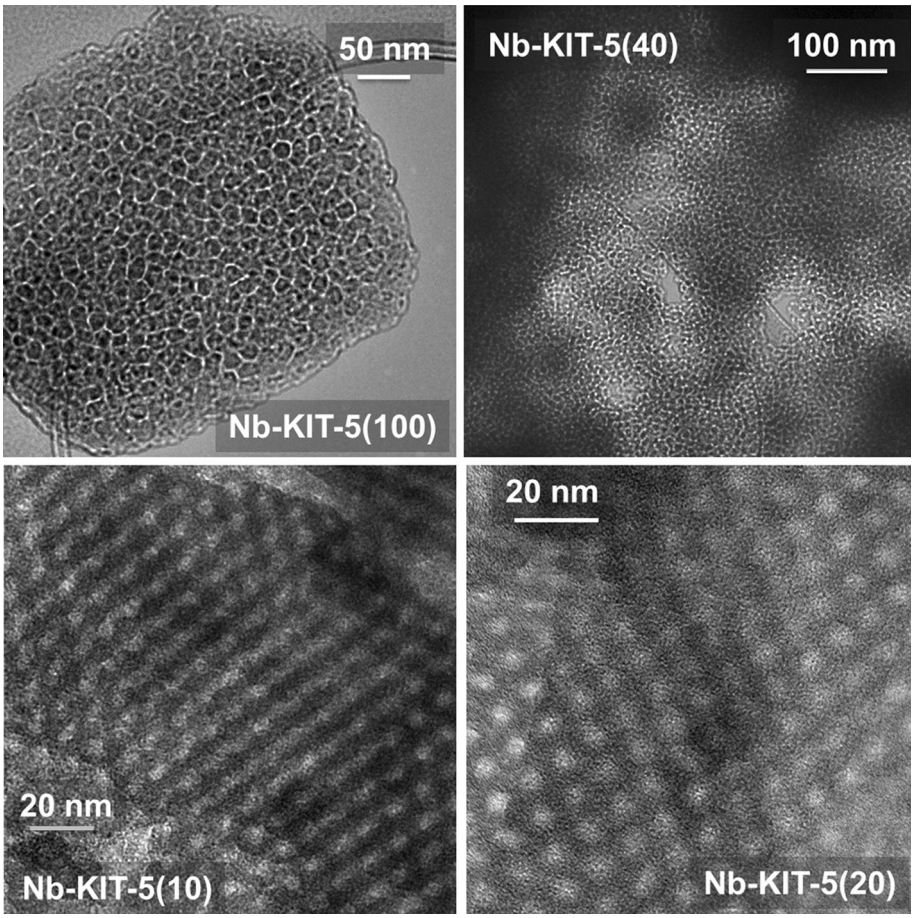

Fig. 4 Representative transmission electron microscopy image of Nb-KIT-5

tetrahedra with low coordination number [11, 28]. Additionally, this band was also attributed to LMCT of oxygen and Nb(V) centers in tetrahedral coordination [29]. In summary, the Nb is predominantly framework-incorporated in the KIT-5 silica matrix with minimal, if any, formation of crystalline Nb_2O_5.

H_2-TPR (temperature programmed reduction) results are summarized in Fig. S3 in ESM. Although the physical admixture of Nb_2O_5 (7 wt%) and KIT-5 show reduction peaks around 892 °C with a shoulder at 793 °C due to reduction of Nb_2O_5 species, Nb-KIT-5 samples with similar Nb content did not show any appreciable hydrogen

consumption confirming the absence of bulk Nb_2O_5 in these materials [23]. This further lends credence to the DR-UV–Vis results that suggest that the Nb is mainly incorporated in the framework.

Nitrogen sorption isotherms of Nb-KIT-5 and neat Si-KIT-5 samples show type IV adsorption isotherm with inflexion points occurring between 0.58 and 0.71 P/P_0 (Fig. 3) due to capillary condensation in the mesopores. The presence of cage-type mesopores is inferred from the broad H2-type hysteresis loop with desorption occurring at $\sim$0.47 P/P_0 [13, 16, 18]. The textural properties of these samples are summarized in Table 1. The specific surface area of Nb-KIT-5 samples decreases from 1022 to 810 $m^2\ g^{-1}$ as the Nb content is increased from 1.4 to 10 wt%, respectively. The corresponding change in the pore volume is relatively minor. The marginal increase in the total pore volume for Nb-KIT-5(10) may be due to a decrease in long range ordering as evidenced from SAXS. The pore size distribution, determined using NLDFT adsorption branch kernel (Autosorb software, NovaWin version 11.0) developed for silicas that exhibit cylindrical/spherical pore geometry, reveals a bimodal pore size distribution typical of cage-type materials (right frame of Fig. 3). The peak around 2.5–2.6 nm corresponds to the mesopore entrance channel size while the 8.8 nm peak corresponds to the cage diameter.

Representative transmission electron microscopy images for Nb-KIT-5 samples are shown in Fig. 4. Cubic

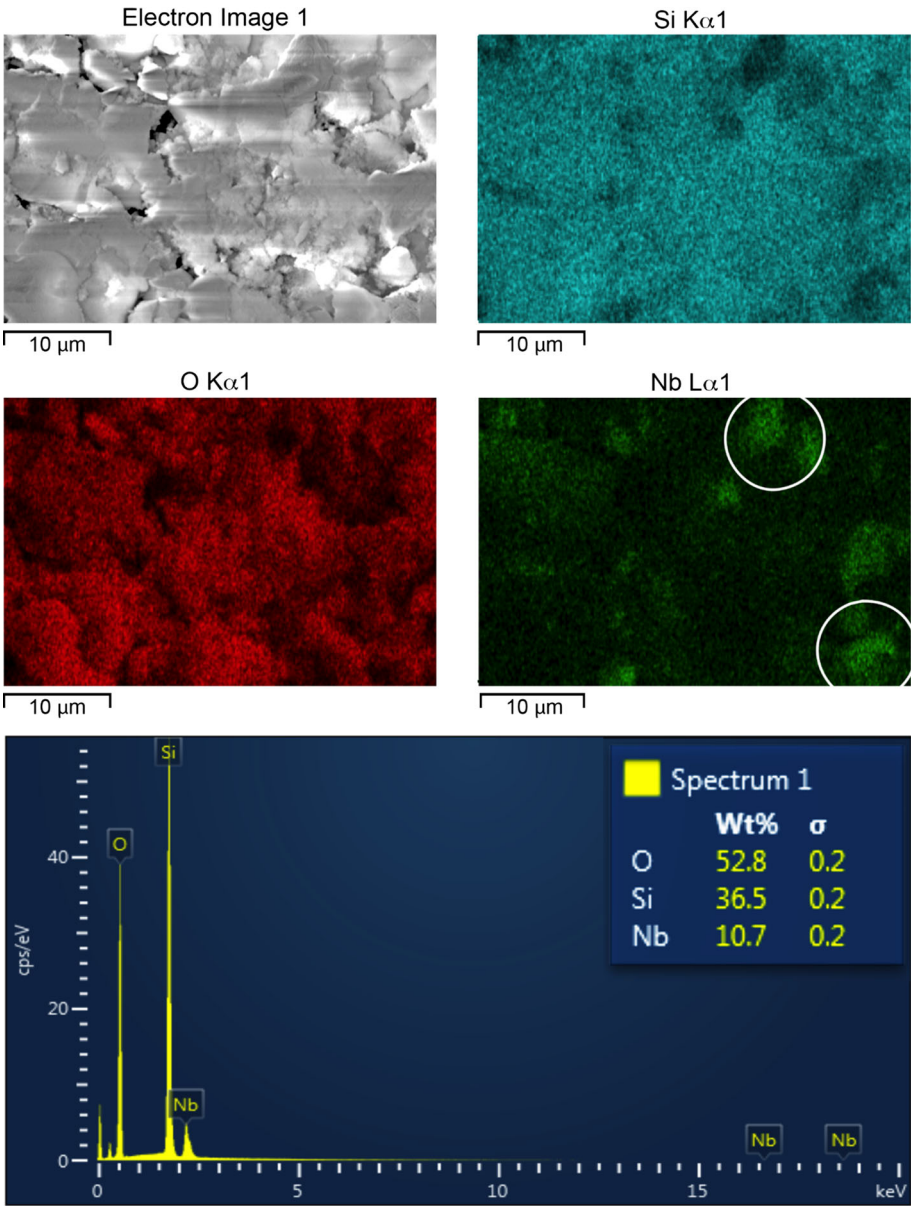

Fig. 5 SEM image, elemental mapping and EDX spectrum of Nb-KIT-5(10). The *circled area* shows Nb-rich regions in the SEM image

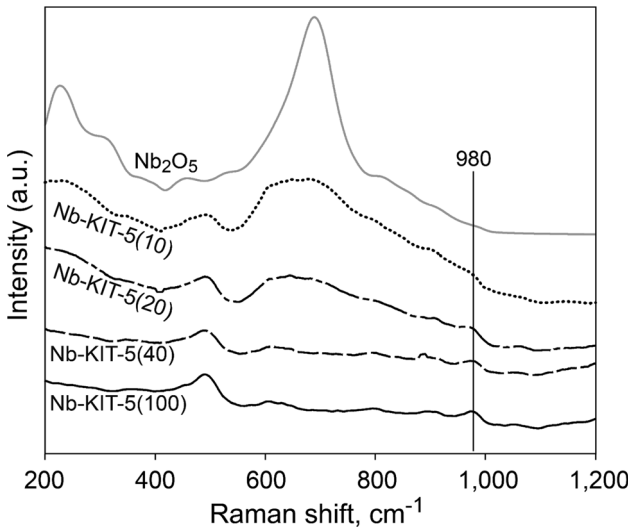

Fig. 6 Raman spectra of Nb-KIT-5(Si/Nb) samples compared with bulk Nb_2O_5

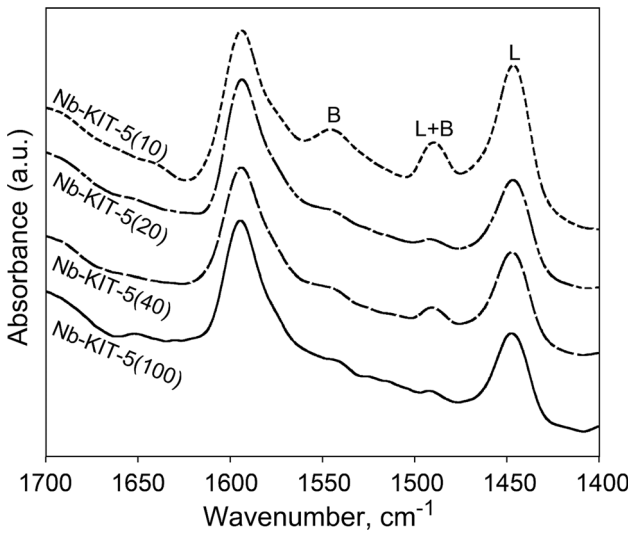

Fig. 7 FTIR spectra of adsorbed pyridine over Nb-KIT-5 (Si/Nb) samples at 120 °C

three-dimensional mesoporous structure with a high degree of long-range ordering is evident from these images. A line profile across the unoriented TEM image yields an average cage pore size of 7.3 nm. A nearly homogeneous distribution of Nb species with a few Nb-rich clusters (Fig. 5) is observed in the elemental mapping of the SEM image of Nb-KIT-5(10) sample. A similar observation was also reported for Nb-KIT-6(10) sample [11]. The Nb content estimated from EDX analysis is close to that from ICP analysis.

Raman spectra of the Nb-KIT-5 samples are presented in Fig. 6. The Nb-KIT-5 samples show a discernible Raman band at 980 cm^{-1} corresponding to highly distorted

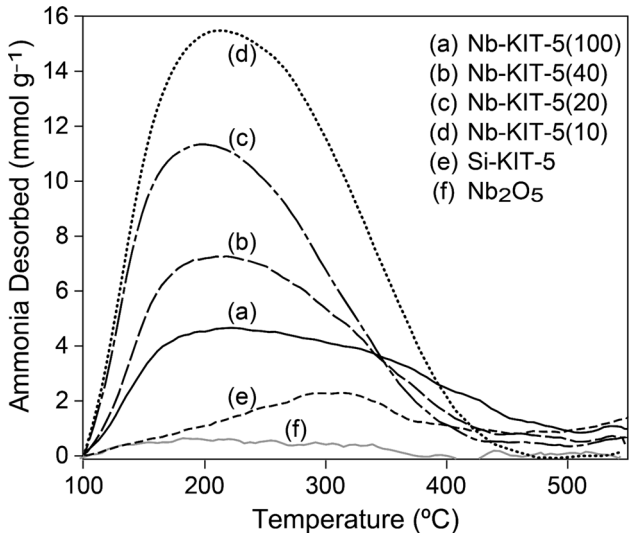

Fig. 8 Temperature programmed desorption of ammonia over Nb-KIT-5(Si/Nb) samples compared with Si-KIT-5 and bulk commercial Nb_2O_5

NbO_6 octahedra sites responsible for imparting Lewis acidity [11, 30]. The broad Raman bands between 600 and 750 cm^{-1}, clearly seen on all except the Nb-KIT-5(100) sample, is attributed to slightly distorted octahedral NbO_6 species that are responsible for Brønsted acid sites [11, 30]. The presence of both Brønsted and Lewis acid sites is further confirmed from FTIR spectra of adsorbed pyridine (Fig. 7). The large peak around 1447 cm^{-1} (denoted as 'L') is attributed to Lewis acid site while the rather weak band at 1545 cm^{-1} (denoted as 'B') is due to Brønsted acid sites. The intensities of the Lewis (L) and Brønsted (B) sites and their ratios (L/B) at various Nb loadings are given in Table 2. Clearly, the Brønsted acidity of the Nb-KIT-5(10) sample increases quite dramatically compared to the other samples. NH_3-TPD results (Fig. 8 and Table 2) show that the total number of acid sites increases with Nb content, similar to the trends reported previously for Nb-KIT-6 [11]. Further, deconvolution of the spectra suggests that the majority of acid sites are present in the medium strength region (250–350 °C), similar to Nb-KIT-6 [11]. Based on the foregoing discussion, the hypothesized structure of different Nb species are given in Scheme 1.

3.2 Epoxidation Activity of Nb-KIT-5

The Nb-KIT-5 materials were tested for styrene epoxidation with H_2O_2 as oxidant and methanol as solvent. The main products detected are benzaldehyde and styrene oxide, which further reacts with methanol (solvent) yielding (1,2-dimethoxyethyl)benzene (1,2-DMEB) as the main product (Scheme 2). Minor reaction products include benzaldehyde dimethyl acetal, phenylacetaldehyde,

Table 2 Acidities of Nb-KIT-5 samples

Sample	Nb (wt%)	Lewis (L)[a]	Brønsted (B)[a]	L/B ratio[b]	Total acidity (NH_3 mmol g^{-1})
Nb-KIT-5(100)	1.4	1.36	0.03	88	0.11
Nb-KIT-5(40)	3.3	1.45	0.04	76	0.14
Nb-KIT-5(20)	5.6	1.48	0.05	62	0.21
Nb-KIT-5(10)	10	2.24	0.27	17	0.33

[a] Relative area

[b] Calculated using absorption coefficients (bands at 1461 and 1454 cm^{-1}, $\varepsilon = 0.165$ cm μmol^{-1}; band at 1545 cm^{-1}, $\varepsilon = 0.078$ cm μmol^{-1})

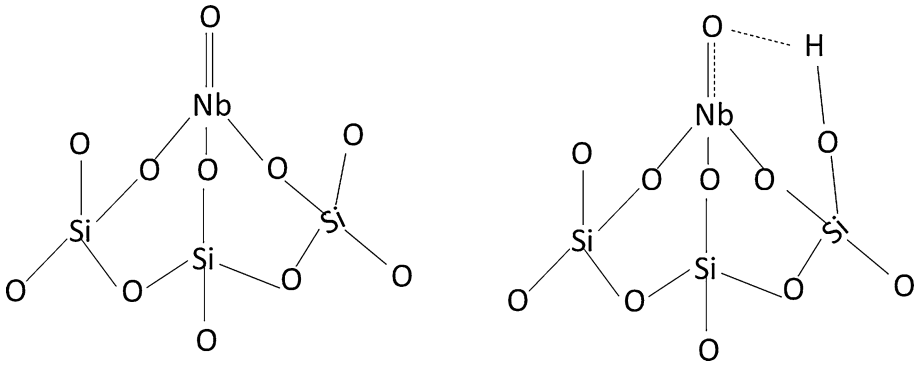

Scheme 1 Isolated $[NbO_4]^-$ site on *left* attributed to Lewis acid sites and Nb^{5+} center on the *right* attributed to Brønsted acid sites. It is hypothesized that interaction of Nb^{5+} center with H_2O also creates Brønsted acid sites [5, 29]

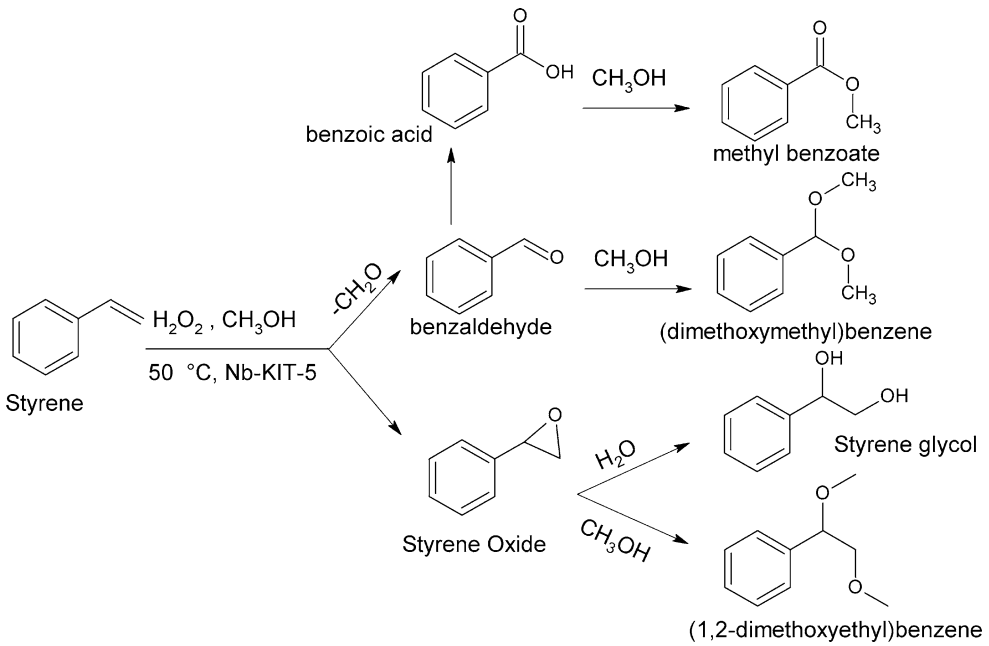

Scheme 2 Observed styrene epoxidation products over Nb-KIT-5 catalysts

methylester of benzoic acid and styrene glycol and are grouped as 'others' in the tables. We also investigated acetone and acetonitrile as solvents in which the substrate and aqueous H_2O_2 are soluble. Results of 6 h batch runs at 50 °C are summarized in Table 3. Styrene conversion is highest with methanol followed by acetonitrile and acetone. While styrene oxide is the primary product with methanol (64 % selectivity with 51 % observed as methylesters), benzaldehyde is the major product with either acetonitrile or acetone. Moreover, the yield of

Table 3 Solvent effects during styrene epoxidation with H_2O_2 over Nb-KIT-5(10)

Solvent	$X_{styrene}$ (%)	S_{PhCHO} (%)	S_{SO} (%)	$S_{1,2\text{-DMEB}}$ (%)
Methanol	51	31	13	51
Acetonitrile	35	65	23	–
Acetone	12	55	24	–

Reaction conditions styrene = 2 mmol, H_2O_2 = 4 mmol, Nb-KIT-5(10) = 20 mg (~10 wt% of styrene), solvent = 3 ml, t = 6 h, T = 50 °C. The minor products include phenylacetaldehyde, benzoic acid, styrene glyclol

Table 5 Effect of H_2O_2 concentration on styrene epoxidation over Nb-KIT-5(10)

$n_{H2O2}/n_{Styrene}$	$X_{styrene}$ (%)	S_{PhCHO} (%)	S_{SO} (%)	$S_{1,2\text{-DMEB}}$ (%)
1	33	35	14	47
2	51	31	13	51
3	74	28	11	52

Reaction conditions styrene = 2 mmol, Nb-KIT-5(10) = 20 mg (~10 wt% styrene), methanol = 3 ml, t = 6 h, T = 50 °C

phenylacetaldehyde in acetonitrile (~8 %) and acetone (~20 %) media suggests isomerization of styrene oxide possibly due to the acidity of Nb-catalysts.

The effect of Nb content on the relative activity and selectivity of Nb-KIT-5 materials in methanol are summarized in Table 4. For identical catalyst weight, the overall styrene TOF (last column, Table 4) increases when normalized with the Nb content. The fact that the styrene TOF does not scale with Nb content suggests that not all the Nb sites are active for the reaction. Interestingly, no significant variation in the product selectivities is observed. The lower styrene conversion rate at higher Nb loadings, Nb-KIT-5(10), is attributed to the presence of a larger fraction of oligomeric NbO_x species that are less active compared to isolated NbO_4 sites. Blank experiments without any catalyst and with only bulk (i.e., crystalline) Nb_2O_5 yielded styrene conversion less than 5 % even after 24 h. The styrene conversion increased linearly with even a mild increase in the number of Lewis acid sites up to a Nb loading of 5.6 wt% (Fig. S4 in ESM) suggesting that the nature of Nb species is similar in catalysts with 1.4–5.6 wt% Nb loading. In addition, at lower Nb loading, the progressively higher styrene TOFs correlate with a higher fraction of framework-incorporated Nb sites observed on such samples. This suggests that framework Nb species is a major contributor to the observed epoxidation activity. It should also be noted that H_2O_2 conversion increased with Nb content and scales linearly up to 5.6 wt% Nb (Fig. S4 in ESM).

No significant changes in either styrene conversion or product selectivities are noted for three consecutive runs (Fig. S5 in ESM) with the recovered catalyst being reactivated by simple calcination in air at 500 °C. In addition, ICP-OES analysis of the spent catalyst revealed low Nb loss (2–5 %), suggesting that these catalysts are stable at the reaction conditions.

When, the H_2O_2/styrene molar ratio is varied from 1 to 3 at 50 °C on a Nb-KIT-5(10) catalyst, the styrene conversion increases from 33 to 54 % (Table 5). This might indicate that the local styrene and H_2O_2 concentrations within the pores might be different than the bulk. Interestingly, the combined styrene oxide and 1,2-DMEB selectivities are found to be similar at the three initial H_2O_2/styrene molar ratios studied (Table 5), suggesting that the reaction orders for these parallel reactions (epoxidation and oxidation of styrene) are similar.

Temporal styrene conversion and selectivity profiles at various temperatures over Nb-KIT-5(10) are given in Fig. 9. When the temperature is increased from 40 to 50 °C, styrene conversion increases from ~29 to ~51 % at the end of 6 h. A further increase in temperature to 60 °C resulted in only a marginal increase in styrene conversion (~58 %). The fact that both styrene oxide and benzaldehyde are formed in similar quantities suggests that

Table 4 Effect of Nb content on styrene epoxidation over Nb-KIT-5(Si/Nb)

Catalyst	Nb (wt%)	$X_{styrene}$ (%)	$X_{H_2O_2}$ (%)[b]	S_{PhCHO} (%)	S_{SO} (%)	$S_{1,2\text{-DMEB}}$ (%)	Productivity ($mmol_{sty}$ $mmol_{Nb}^{-1}$ h^{-1})
Nb-KIT-5(10)	10	51	72	31	13	51	7.9
Nb-KIT-5(20)	5.6	43	65	31	13	50	11.9
Nb-KIT-5(40)	3.3	39	63	30	11	53	18.3
Nb-KIT-5(100)	1.4	32	52	29	13	52	35.4
Blank[a]	–	<5	–	–	–	–	–
Crystalline Nb_2O_5[a]	–	<5	–	–	–	–	–
Si-KIT-5[a]	–	No reaction	–	–	–	–	–

Reaction conditions: styrene = 2 mmol, H_2O_2 = 4 mmol, catalyst = 20 mg (~10 wt% of styrene), methanol = 3 ml, t = 6 h, T = 50 °C

[a] t = 24 h

[b] H_2O_2 converted was measured by ceric sulfate titration

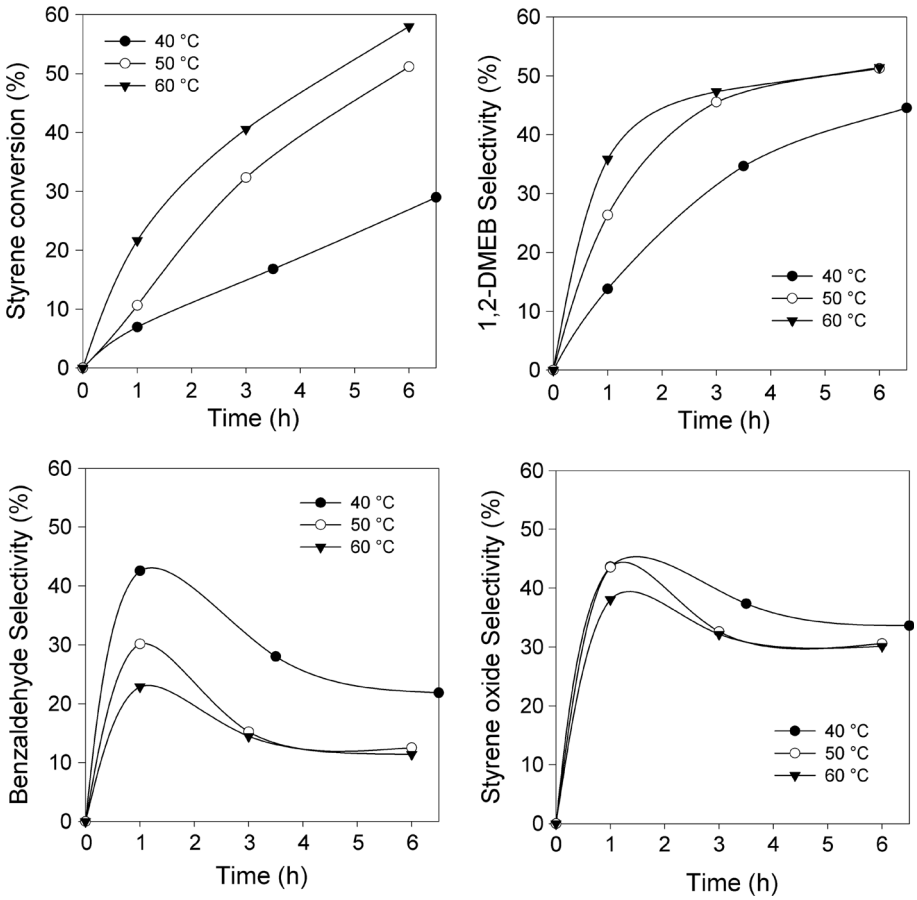

Fig. 9 Conversion-time profile for epoxidation of styrene at various temperatures over Nb-KIT-5(10). Reaction conditions: styrene = 2 mmol, H_2O_2 = 4 mmol, Nb-KIT-5(10) = 20 mg (~10 wt% of styrene), methanol = 3 ml

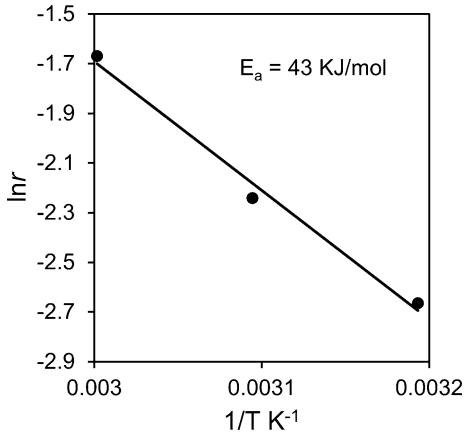

Fig. 10 Estimate of overall activation energy for styrene conversion

both epoxide formation and the C=C cleavage reactions are competitive. The selectivities of both these primary products pass through a maximum suggesting that they undergo further reaction. In particular, the selectivity of 1,2-DMEB increases with both temperature and time. Regardless of temperature, a combined selectivity of ~63 % towards styrene oxide and 1,2-DMEB was observed, clearly suggesting that the loss of styrene oxide selectivity is due to successive reaction with methanol. A moderate activation energy of 43 kJ mol^{-1} is estimated for the overall reaction from a plot of ln *r* (considering the conversion after 1 h) and 1/T (Fig. 10).

We also compared the catalytic activity of different Nb-incorporated mesoporous catalysts (Nb incorporated into KIT-5, SBA-15, MCM-41 and MCM-48), all synthesized in our lab, for styrene epoxidation at 50 °C for 6 h and the results are summarized in Table 6. The styrene conversion followed the order KIT-5 > KIT-6 ≈ SBA-15 > MCM-48. The lower conversion on MCM-41 catalyst may be attributed to lower amounts of Nb content in the catalyst. A uniformly distributed Nb-MCM-41 sample with a similar Nb loading (as the other Nb-based catalysts) could not be prepared since the higher Nb loading resulted in a mixture of amorphous and MCM-41 type material.

It is also interesting to note that in all these catalysts 1-2-DMEB was observed as major product except MCM-41 catalyst. Clearly, the cubic mesostructured catalysts perform better than the two-dimensional mesostructured catalysts.

Table 6 Effect of Nb content on styrene epoxidation over Nb-KIT-5(Si/Nb)

Catalyst (Si/Nb)	Nb (wt%)	$X_{styrene}$ (%)	S_{PhCHO} (%)	S_{SO} (%)	$S_{1,2\text{-DMEB}}$ (%)
Nb-KIT-5(20)	5.6	43	31	13	50
Nb-KIT-6(20)[a]	6.8	32	21	8	65
Nb-MCM-41(50)[b]	3.0	12	42	48	9
Nb-MCM-48(25)[c]	5.0	25	18	14	56
Nb-SBA-15(20)[d]	6.2	31	24	7	64

Reaction conditions styrene = 2 mmol, H_2O_2 = 4 mmol, catalyst = 20 mg (~10 wt% of styrene), methanol = 3 ml, t = 6 h, T = 50 °C

[a] Prepared according to Ref. [11]

[b] Prepared according to Ref. [31] but $NbCl_5$ was used as Nb-source

[c] Prepared according to Ref. [32] but $NbCl_5$ was used as Nb-source

[d] Prepared according to Ref. [22]

4 Conclusions

In summary, a series of Nb-containing cage type mesoporous KIT-5 materials were synthesized by direct hydrothermal synthesis method under acidic conditions. The cubic ordered pores were confirmed by SAXS, N_2 sorption and HR-TEM results. Diffuse reflectance UV–Vis and Raman spectra confirm the presence of isolated NbO_4 and oligonuclear NbO_x species, with the extraframework oxide species being favored at higher Nb loadings. No crystalline Nb_2O_5 was detectable as confirmed by XRD and H_2-TPR results. Nb incorporation creates both Lewis and Brønsted sites that are tuned with Nb loading. The Nb-KIT-5 materials show significant and stable styrene epoxidation activity in methanol with H_2O_2 as oxidant. The framework Nb species rather than the extraframework niobium oxide species appear to be primarily responsible for the observed epoxidation activity. In addition to being a favored solvent, the use of methanol also enables the formation of the dimethyl ether of styrene glycol in one step.

Acknowledgments This research was partly supported with funds from the following sources: National Science Foundation Accelerating Innovation Research Grant (IIP-1127765) and United States Department of Agriculture USDA/NIFA Award 2011-10006-30362. The authors thank Dr. Prem Thapa of the Microscopy and Analytical Imaging Laboratory, University of Kansas for dual beam SEM and TEM characterizations and Dr. Brian P. Grady, University of Oklahoma, for SAXS analysis. The FEI Versa 3D dual-beam FIB/SEM instrument and WAXS analysis instrument (XRD) at the University of Kansas was acquired through an NSF Major Research Instrumentation grants CBET 1229645 and CHE-0923449 respectively.

References

1. Kholdeeva OA (2014) Recent developments in liquid-phase selective oxidation using environmentally benign oxidants and mesoporous metal silicates. Catal Sci Technol 4:1869–1889
2. Feliczak-Guzik A, Nowak I (2009) Mesoporous niobosilicates serving as catalysts for synthesis of fragrances. In: Selective papers of the 6th international symposium group five elements, Poznan, Poland, 7–10 May 2008, vol 142, pp 288–292
3. Somma F, Strukul G (2006) Niobium containing micro-, meso- and macroporous silica materials as catalysts for the epoxidation of olefins with hydrogen peroxide. Catal Lett 107:73–81
4. Aronne A, Turco M, Bagnasco G et al (2008) Gel derived niobium–silicon mixed oxides: characterization and catalytic activity for cyclooctene epoxidation. Appl Catal Gen 347:179–185
5. Tiozzo C, Bisio C, Carniato F et al (2013) Niobium-silica catalysts for the selective epoxidation of cyclic alkenes: the generation of the active site by grafting niobocene dichloride. Phys Chem Chem Phys 15:13354–13362
6. Tiozzo C, Bisio C, Carniato F et al (2013) Epoxidation with hydrogen peroxide of unsaturated fatty acid methyl esters over Nb(V)-silica catalysts. Eur J Lipid Sci Technol 115:86–93
7. Gallo A, Tiozzo C, Psaro R et al (2013) Niobium metallocenes deposited onto mesoporous silica via dry impregnation as catalysts for selective epoxidation of alkenes. J Catal 298:77–83
8. Tiozzo C, Bisio C, Carniato F, Guidotti M (2014) Grafted non-ordered niobium-silica materials: versatile catalysts for the selective epoxidation of various unsaturated fine chemicals. Catal Today 235:49–57
9. Nowak I, Kilos B, Ziolek M, Lewandowska A (2003) Epoxidation of cyclohexene on Nb-containing meso- and macroporous materials. Catal Today 78:487–498
10. Di Serio M, Turco R, Pernice P et al (2012) Valuation of Nb2O5–SiO2 catalysts in soybean oil epoxidation. Catal Today 192:112–116
11. Ramanathan A, Maheswari R, Barich DH, Subramaniam B (2014) Niobium incorporated mesoporous silicate, Nb-KIT-6: synthesis and characterization. Micropor Mesopor Mater 190:240–247
12. Yan W, Ramanathan A, Ghanta M, Subramaniam B (2014) Towards highly selective ethylene epoxidation catalysts using hydrogen peroxide and tungsten- or niobium-incorporated mesoporous silicate (KIT-6). Catal Sci Technol 4:4433–4439
13. Kleitz F, Liu D, Anilkumar GM et al (2003) Large cage face-centered-cubic *Fm3m* mesoporous silica: synthesis and structure. J Phys Chem B 107:14296–14300
14. Maheswari R, Pachamuthu MP, Ramanathan A, Subramaniam B (2014) Synthesis, characterization, and epoxidation activity of tungsten-incorporated SBA-16 (W-SBA-16). Ind Eng Chem Res. doi:10.1021/ie501784c
15. Anand C, Srinivasu P, Mane GP et al (2013) Direct synthesis and characterization of highly ordered cobalt substituted KIT-5 with 3D nanocages for cyclohexene epoxidation. Micropor Mesopor Mater 167:146–154

16. Anand C, Srinivasu P, Mane GP et al (2012) Preparation of mesoporous titanosilicate molecular sieves with a cage type 3D porous structure for cyclohexene epoxidation. Micropor Mesopor Mater 160:159–166
17. Srinivasu P, Alam S, Balasubramanian VV et al (2008) Novel three dimensional cubic *Fm3m* mesoporous aluminosilicates with tailored cage type pore structure and high aluminum content. Adv Funct Mater 18:640–651
18. Ramanathan A, Maheswari R, Grady BP et al (2013) Tungsten-incorporated cage-type mesoporous silicate: W-KIT-5. Micropor Mesopor Mater 175:43–49
19. Hsu YT, Chen WL, Yang CM (2009) Co-condensation synthesis of aminopropyl-functionalized KIT-5 mesophases using carboxy-terminated triblock copolymer. J Phys Chem C 113:2777–2783
20. Wu CY, Hsu YT, Yang CM (2009) Structural modulation of cage-like mesoporous KIT-5 silica by post-synthesis treatments with ammonia and/or sulfuric acid. Micropor Mesopor Mater 117:249–256
21. Balasubramanian VV, Srinivasu P, Anand C et al (2008) Highly active three-dimensional cage type mesoporous aluminosilicates and their catalytic performances in the acetylation of aromatics. Micropor Mesopor Mater 114:303–311
22. Trejda M, Tuel A, Kujawa J et al (2008) Niobium rich SBA-15 materials—preparation, characterisation and catalytic activity. Micropor Mesopor Mater 110:271–278
23. Carniti P, Gervasini A, Marzo M (2008) Dispersed NbOx catalytic phases in silica matrixes: influence of niobium concentration and preparative route. J Phys Chem C 112:14064–14074
24. Hartmann M (1999) Synthesis of niobium- and tantalum-containing silicalite-1. Chem Lett 5:407–408
25. Ko YS, Jang HT, Ahn WS (2007) Hydrothermal synthesis and characterization of niobium-containing silicalite-1 molecular sieves with MFI structure. J Ind Eng Chem 13:764–771
26. Hartmann M, Prakash AM, Kevan L (2003) Characterization and catalytic evaluation of mesoporous and microporous molecular sieves containing niobium. Catal Today 78:467–475
27. Srinivasu P, Anand C, Alam S et al (2008) Direct synthesis and the morphological control of highly ordered two-dimensional P6mm mesoporous niobium silicates with high niobium content. J Phys Chem C 112:10130–10140
28. Tanaka T, Nojima H, Yoshida H et al (1993) Preparation of highly dispersed niobium oxide on silica by equilibrium adsorption method. Catal Today 16:297–307
29. Carniato F, Bisio C, Psaro R et al (2014) Niobium(V) saponite clay for the catalytic oxidative abatement of chemical warfare agents. Angew Chem Int Ed 53:10095–10098
30. García-Sancho C, Sádaba I, Moreno-Tost R et al (2013) Dehydration of xylose to furfural over MCM-41-supported niobium-oxide catalysts. ChemSusChem 6:635–642
31. Gallo JMR, Paulino IS, Schuchardt U (2004) Cyclooctene epoxidation using Nb-MCM-41 and Ti-MCM-41 synthesized at room temperature. Appl Catal A 266:223–227
32. Ramanathan A, Maheswari R, Thapa PS, Subramaniam B (2013) Novel materials for catalysis and fuels processing. In: Bravo-Suárez JJ, Kidder MK, Schwartz V (eds) Rapid room temperature synthesis of Ce-MCM-48: an active catalyst for trans-stilbene epoxidation with tert-butyl hydroperoxide. ACS Symposium Series 1132, American Chemical Society. Washington, DC, pp 213–228. doi:10.1021/bk-2013-1132.ch008